Relativistic mean field calculations in neutron-rich nuclei

Cite as: AIP Conference Proceedings **1609**, 63 (2014); https://doi.org/10.1063/1.4893254
Published Online: 17 February 2015

G. Gangopadhyay, Madhubrata Bhattacharya, and Subinit Roy

Relativistic Mean Field Calculations in Neutron-rich Nuclei

G. Gangopadhyay*, Madhubrata Bhattacharya* and Subinit Roy†

*Department of Physics, University of Calcutta
92 Acharya Prafulla Chandra Road, Kolkata 700 009, India
†Saha Institute of Nuclear Physics, Block AF, Sector 1, Kolkata- 700 064, India

Abstract. Relativistic mean field calculations have been employed to study neutron rich nuclei. The Lagrange's equations have been solved in the co-ordinate space. The effect of the continuum has been effectively taken into account through the method of resonant continuum. It is found that BCS approximation performs as well as a more involved Relativistic Continuum Hartree Bogoliubov approach. Calculations reveal the possibility of modification of magic numbers in neutron rich nuclei. Calculation for low energy proton scattering cross sections shows that the present approach reproduces the density in very light neutron rich nuclei.

Keywords: Relativistic mean field, Resonant continuum, Binding energy, Scattering
PACS: 2.160.Jz, 21.10.Dr, 25.40.Cm

1. INTRODUCTION

In the last two decades, giant leaps in detection systems and accelerator technologies, particularly with the availability of radioactive ion beams, have made nuclear physics an exciting subject. Old theories have been severely tested as never before in explaining the new data. The limits of nuclear stability are now being probed and yielding surprising results. Major surprises in low-energy nuclear structure include the disappearance of the normal shell closures observed near the stability valley along with the emergence of new magic numbers and neutron haloes in nuclei very close to the neutron drip line.

Relativistic mean field (RMF) approach has proved to be very successful in explaining different features of stable and exotic nuclei such as ground state binding energy, deformation, radius, excited states, spin-orbit splitting, neutron halo, etc[1]. In nuclei far away from the stability valley, the single particle level structure undergoes drastic changes in which the spin-orbit interaction plays an important role. Being based on the Dirac Lagrangian density, and thus naturally incorporating the spin degree of freedom, RMF is particularly suited to investigate these nuclei. Thus, neutron rich nuclei can be fruitfully investigated within RMF formalism.

2. THEORY

RMF calculations are well known. Interested readers are referred to excellent reviews that have been published in recent years. In the conventional RMF+BCS approach for even-even nuclei, the Euler-Lagrange equations are solved under the assumptions of classical meson fields, time reversal symmetry, no-sea contribution, etc. Pairing is introduced under the BCS approximation.

In this approach, nucleons interact via exchange of a number of mesons. There are different variations of the Lagrangian density as well as a number of different parametrizations. We have employed the densities NLSH[2], NL3[3], NL2[4] and FSU Gold[5] Lagrangian density. The last one contains, apart from the usual component describing a system of nucleons interacting via exchange of mesons, nonlinear terms involving self coupling of the scalar-isoscalar and the vector-isoscalar meson, as well as coupling between the vector-isoscalar meson and the vector-isovector meson.

The usual practice of solving the mean field equations is to expand them in a harmonic oscillator basis cannot explain the density of halo nuclei near the drip line because of slow convergence in the asymptotic region. Hartree Fock Bogoliubov (HFB) and Relativistic Hartree Bogoliubov (RHB) methods in coordinate space have emerged as two very accurate approaches of treating the nuclei very close to the drip line. The effect of the states in the continuum is usually incorporated by solving the equations in coordinate space using the box normalization condition, thus replacing the continuum with a set of discrete positive energy states. In nuclei near the stability valley, this procedure works well, because the continuum states being far away from the Fermi level, their contributions are small. However, in neutron rich nuclei near the drip line, the Fermi level is very close to the continuum and the positive energy states are expected to affect the results significantly. In this situation the application of the box normalization procedure is open to question. Besides, in this procedure, the single particle energy levels depend on the size of the box chosen, introducing an unwelcome feature.

Frontiers in Gamma-Ray Spectroscopy 2012 - FIG12
AIP Conf. Proc. 1609, 63-70 (2014); doi: 10.1063/1.4893254

We intend to study neutron rich nuclei in an approach that includes the effect of the resonant continuum. Non-relativistic Hartree Fock[6, 7] and RMF equations[8, 9] involving continuum states have been solved with exact boundary conditions taking into account the width of the continuum levels.

The nucleons are represented by Dirac spinors

$$\psi_\kappa = \frac{1}{r}\begin{pmatrix} iG(r)\Phi_\kappa \\ F(r)\Phi_{-\kappa}\end{pmatrix}\eta_t \tag{1}$$

where η is the isospin operator. In the co-ordinate space approach, the simultaneous radial equations for $G(r)$ and $F(r)$ are usually solved in the case of the bound state by assuming the wave function vanishes at large distance. For the continuum, we have assumed scattering type boundary conditions. At large distance, where both the scalar and vector field vanish, the solution for neutron states is sought for scattering type boundary conditions, *viz.*,

$$\begin{aligned} G_\kappa(r) &= C\alpha r[cos\delta_l j_l(\alpha r) - sin\delta_l \eta_l(\alpha r)] \\ F_\kappa(r) &= C\frac{\alpha^2 r}{E+M}[cos\delta_l j_{l-1}(\alpha r) - sin\delta_l \eta_{l-1}(\alpha r)] \end{aligned} \tag{2}$$

where $\alpha^2 = E^2 - M^2$ and j_l and η_l are Bessel and Neumann functions, respectively. The phase shift associated with the spinor functions is given by δ_l. As is well known, the quantum number κ associated with angular momentum l by the relation

$$\begin{aligned} \kappa = -(l+1) \text{ if } j = l+1/2 \\ \kappa = +l \text{ if } j = l-1/2 \end{aligned}$$

The energy of a resonant state is determined by the condition that the phase shift is $\pi/2$. The phase shift δ_l is obtained by matching conditions at an appropriately large radius where the scalar and vector fields vanish. The wave function of the normalized state is normalized to a delta function $\delta(E-E')$ which results in

$$C_\nu = \sqrt{\frac{M+E}{2\alpha\pi}}$$

In the vicinity of a resonance, the radial wave functions of a scattering states are largely localized inside the nucleus.

In the vicinity of an isolated resonance, the level density depend on the derivative of the phase shift

$$g_l(E) = \frac{2j_l+1}{\pi}\frac{d\delta_l}{dE} = \frac{2j_l+1}{\pi}\frac{\Gamma_l/2}{(E_l-E)^2+\Gamma_l^2/4} \tag{3}$$

where Γ and E_l are the width and energy of the resonance.

The BCS calculation is performed for a delta interaction, *i.e.* $V = V_0\delta(\vec{r}_1 - \vec{r}_2)$. The usual BCS equations now contain both the bound states as well as the resonant continuum. The equations involving these states are referred as resonant-BCS (rBCS) equations. They are

$$\begin{aligned} \Delta_i = \sum_j V_{i\bar{i},j\bar{j}} u_i v_j + \sum_\nu V_{i\bar{i},\nu\varepsilon_\nu\overline{\nu\varepsilon_\nu}} \\ \int_{I_\nu} g_\nu(\varepsilon) u_\nu(\varepsilon) v_\nu(\varepsilon) d\varepsilon \end{aligned} \tag{4}$$

$$\begin{aligned} \Delta_\nu = \sum_j V_{\nu\varepsilon_\nu\overline{\nu\varepsilon_\nu},j\bar{j}} u_j v_j + \sum_\mu V_{\nu\varepsilon_\nu\overline{\nu\varepsilon_\nu},\mu\varepsilon_\mu\overline{\mu\varepsilon_\mu}} \\ \int_{I_\nu} g_\mu(\varepsilon') u_\mu(\varepsilon') v_\mu(\varepsilon') d\varepsilon' \end{aligned} \tag{5}$$

$$N = \sum_i {V_i}^2 + \sum_\nu \int_{I_\nu} g_\nu^c(\varepsilon) v_\nu^2(\varepsilon) d\varepsilon \tag{6}$$

where $ij(\mu\nu)$ refer to bound (continuum) states. The range of the integral over energy for the ν-th state is given by I_ν.

With the rBCS equations being solved for obtaining the occupational probabilities, the baryon density in the Lagrange's equations become

$$\begin{aligned} \rho_b(r) = \sum_i \frac{2j_i+1}{4\pi} {v^2}_i D_{1i}(r) \\ + \sum_\nu \frac{2j_\nu+1}{4\pi}\int_{I_\nu} g_\nu(\varepsilon_\nu) {v^2}_\nu(\varepsilon_\nu) D_{1\nu}(r) d\varepsilon_\nu \end{aligned} \tag{7}$$

$$\tag{8}$$

Here, we have written $D_{1i}(r) = \mid G_i(r) \mid^2 + \mid F_i(r) \mid^2$. Similar expressions occur for other densities also. Thus, one can see the contribution from the resonant continuum explicitly in the last two equations.

One can solve the Dirac equation for the nucleon and the Klein Gordon equations for the meson fields with the densities defined above. The total binding energy is written as

$$\begin{aligned} E = \sum_i (2j_i+1) {v^2}_i E_i \\ + \sum_\nu (2j_\nu+1)\int_{I_\nu} g_\nu(\varepsilon_\nu) {v^2}_\nu(\varepsilon_\nu)\varepsilon_\nu d\varepsilon_\nu \\ - \frac{1}{2}\int (g_\sigma\rho_s\sigma_0 + g_\omega + g_\rho\rho_3^0\rho_3 + e\rho_c A_0) d^3r \\ - \int (\frac{g_2\sigma^3}{3} + \frac{g_3\sigma^4}{4}) d^3r - E_{pair} - \frac{3}{4}41A^{-1/3} \end{aligned} \tag{9}$$

where the last term is the centre of mass correction and E_{pair} is the pairing correlation energy given by

$$\begin{aligned} E_{pair} = \sum_i (2j_i+1)\Delta_i u_i v_i \\ + \sum_\nu (2j_\nu+1)\Delta_\nu \int_{I_\nu} g_\nu(\varepsilon_\nu) u_\nu(\varepsilon_\nu) v_\nu(\varepsilon_\nu) d\varepsilon_\nu \end{aligned} \tag{10}$$

The RMF+BCS approach in co-ordinate space was modified to study deformed nuclei also[10]. We have adopted this method to study the deformation of these nuclei. In odd nucleus the last odd nucleon breaks the time reversal symmetry of the system. However, it is well known that the bulk quantities like binding energy or radii are not affected by the breaking of the symmetry. Since we are interested only in these quantities, we have use the tagging approximation to study odd mass nuclei. We have extended our calculations to nuclei beyond the neutron drip line also. The strength of the zero range volume pairing force for neutrons has been from systematics as it was found to explain the trend in binding energy in very light nuclei reasonably well. We have also observed that moderate variations of the pairing strength do not influence the results to any great extent.

3. RESULTS

3.1. Very light nuclei

In Table 1, our results for binding energy and radius values in neutron rich light nuclei are given and compared with experimental measurements wherever available. Here and later the experimental binding energy values are from Ref. [11]. The calculated results are in reasonable agreement with experimental measurements given the fact that the number of nucleons is very small and the mean field approach may not be very accurate.

One of the Lagrangian densities, FSU Gold, predicts the level $\nu p_{1/2}$ to be in the continuum in ^{6}He with a very large with width 1.8 MeV, which, in ^{8}He, comes down to 0.28 MeV. Obviously, the angular momentum of the $p_{1/2}$-state being small, the centrifugal barrier cannot localize the state very effectively. The effect of the resonant level on the binding energy is very small (less than 0.05% in the case of ^{6}He) as the occupancy of $p_{1/2}$ level is very small. However, even this small occupancy has a larger effect on the neutron radius concerned, because an unbound resonant level has a radius much larger than the bound state. Thus, we find that the effect of including the effect of the level width increases the neutron radius by 0.5%. Small though the number is, it is comparable to the experimental errors in measurements of rms radii in these nuclei.

The single particle neutron levels in Be are given in Fig. 1. A level inversion occurs with the $2s_{1/2}$ state coming down below the $1d_{5/2}$ state. The former becomes weakly bound in ^{12,14}Be. This inversion is essential for the nucleus ^{14}Be to be bound. However, neither the RMF+BCS scheme, nor the RHB approach can predict the parity inversion in neutron rich Be nuclei, which has been observed in ^{11}Be. This inversion also could not be explained by a full scale shell model calculation[12] and the authors of that work have suggested that the effect of three body forces should be included to explain the phenomenon. Although the RMF forces contain contributions from higher body forces, both the presently used parameterizations, *i.e.* NLSH and NL3 fail in this regard.

TABLE 1. Binding energy and radius in very light isotopes in the spherical approach.

Nucleus		B.E./A (MeV)	Radius (fm)		
			r_p	r_n	r_{rms}
^{6}He	Expt.	4.878	2.068	2.72	2.48
	NL2	5.161	1.89	3.63	3.16
^{8}He	Expt.	3.926	1.929		2.52
	NL2	3.765	1.88	3.69	3.33
^{10}Be	Expt.	6.498			2.30
	NLSH	6.192	2.19	2.42	2.33
^{12}Be	Expt.	5.721			2.59
	NLSH	5.855	2.26	2.73	2.58
^{14}Be	Expt.	4.994			3.16
	NLSH	4.992	2.27	4.04	3.62
^{14}C	Expt.	7.520		2.70	2.30
	NLSH	7.616	2.37	2.56	2.48
^{16}C	Expt.	6.922		2.89	2.70
	NLSH	6.780	2.39	2.93	2.74
^{18}C	Expt.	6.426		3.06	2.82
	NLSH	6.220	2.41	3.04	2.84
^{20}C	Expt.	5.959			2.98
	NLSH	5.843	2.43	3.16	2.96
^{22}C	Expt.	5.440*			
	NLSH	5.568	2.45	3.38	3.15

* Estimated value

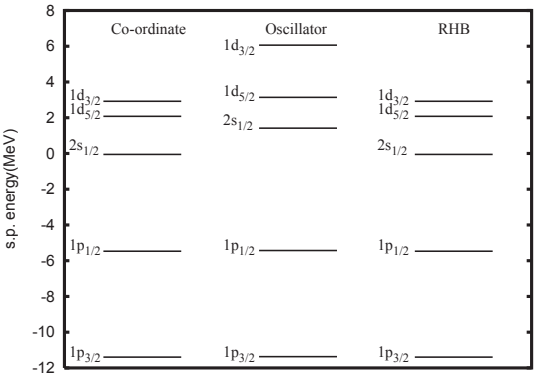

FIGURE 1. Calculated single particle neutron states in ^{14}Be in the spherical approximation. See text for details.

We have also studied the nuclei for deformation in RMF formalism. The nuclei ^{12}Be and ^{14,22}C are found to be spherical in agreement with the fact that the neutron number N=8 and N=16 are magic numbers. In this regard, our calculation agrees with the RHB results of

TABLE 2. Calculated binding energy and deformation(β) in Be and C isotopes. NLSH force has been used.

Nucleus	β_{2p}	β_{2n}	β_2	B.E./A(MeV)
^{10}Be	0.36	0.14	0.23	6.398
	-0.24	-0.16	-0.19	6.365
^{16}C	0.08	0.46	0.32	6.888
	-0.11	-0.24	-0.19	6.879
^{18}C	0.09	0.40	0.30	6.387
	-0.12	-0.39	-0.30	6.381
^{20}C	-0.11	-0.30	-0.25	5.968
	0.04	0.14	0.11	5.865

Lalazissis *et al*[13]. We also have observed ^{14}Be to be spherical. All the other nuclei show varying degree of deformation. The results of our calculation for binding energy and quadrupole deformation after the inclusion of deformation are presented in Table 2. For deformed nuclei, the calculation self-consistently converges to the two coexistent minima, prolate and oblate, according as one starts with a positive or a negative initial deformation. One can see that in all these nuclei, the agreement between the calculated binding energy and experimental measurements improve for deformed solutions. Also, in most cases the proton and neutron deformation are substantially different from each other. In all the deformed nuclei studied, solutions for prolate and oblate deformation are very close in energy. Our results agree with that of the deformed RHB calculation of [13] except in a few cases as discussed. The nucleus ^{10}Be, which has not been studied in Ref. [13], comes out to be strongly deformed. Here, the proton deformation is much larger than the corresponding neutron one. In ^{14}Be, because of the level inversion, the last two neutrons occupy the $2s_{1/2}$ level instead of the deformation driving Ω=5/2 orbital of the $1d_{5/2}$ level as expected from level ordering observed near stability valley. Hence its ground state comes out to be spherical in contrast to Ref. [13], where the ground state is obtained as strongly deformed. In ^{16}C, the prolate and the oblate solutions come out to be nearly degenerate. This was observed in Ref. [13] also. Similarly, in ^{18}C, although the ground state comes out to be prolate, the binding energy of the oblate solution is only about 150 keV less. The nucleus ^{20}C is again observed to be oblate. In contrast, the deformed RHB calculation [13] suggests that both ^{18,20}C are oblate in their ground states. Lalazissis *et al*have noted that because of the close lying self-consistent minima, it is not always possible for the mean field theories to accurately predict the sign of the deformation. In all the deformed C isotopes, proton distribution is very weakly deformed while the neutron distribution, except for the case of the prolate solution in ^{20}C, show moderate to large deformation.

3.1.1. Nuclei beyond the neutron drip line : ^{5,7}He

In ^{5,7}He, the lowest energy states arise out of ground state of the even-even core coupled to a $p_{3/2}$ neutron. In ^{5}He, a recent analysis [14] of an older work[15] found the ground state at a resonance energy of 0.741(4) MeV with width 0.655 MeV. Tilley *et al*[16] placed it at 0.798 MeV with a width 0.648 MeV and found another resonance with spin-parity $1/2^-$ at 2.068 MeV with width 5.57 MeV. Though the results for the ground state resonance was in reasonable agreement with earlier measurements[17], the situation in $1/2^-$ was different. Here, previous work placed the resonance at 4.089 MeV.

Theoretically, we find that ^{5}He is unstable against neutron emission. The lowest state is the $3/2^-$ resonance calculated to be at 0.92 MeV energy, in good agreement with experiment. However, the $1/2^-$ resonance is predicted to be at a resonance energy of 4.47 MeV, at a much higher energy compared with the result of Ref.[16]. Some other theoretical investigations also predict a higher energy resonance for the $1/2^-$ state. For example, continuum shell model calculation of Volya and Zelevensky[18] predicted the $3/2^-$ and the $1/2^-$ resonances at 0.99 MeV and 4.93 MeV, respectively.

In ^{7}He, the $3/2^-$ resonance occurs at a energy of approximately 0.45 MeV and has width $\Gamma = 0.15$ MeV[19]. A resonant state at E^*=2.9 MeV with width around Γ=2 MeV[19] was interpreted as odd nucleon coupled to the 2^+ excited state of the core. Another resonant state at $E^* = 0.6(0.1)$ MeV with Γ=0.75 MeV observed in the breakup of ^{8}He [20] was suggested to arise out of coupling of $p_{1/2}$ nucleon to the ^{6}He ground state. Skaza *et al*[21] observed the $1/2^-$ resonance at $E^* = 0.9(0.5)$ MeV with Γ=1.0 MeV. Indications of a low energy narrow resonance was also observed by other workers[22]. However, a study[23] using isobaric analog states did not observe the last resonance but reported a broad $1/2^-$ resonance at 2.2 MeV. Ryezayeva *et al*[24] also did not find any low energy $1/2^-$ resonance but observed indications of a broad resonance at 1.45 MeV. Wuosmaa *et al*[25, 19] observed a possible resonance at 2.6 MeV excitation energy but no indication of any $1/2^-$ resonance at lower energy. Aksyutina *et al*[14] found the resonance energy of the ground state to be 0.388 (2) MeV and width 0.190 MeV. They could not draw any unambiguous conclusion about the possibility of a resonance around 1 MeV. Our calculations place the $3/2^-$ resonance at 0.63 MeV energy. It appears at a higher energy possibly because the experimental state also has a contribution form $p_{1/2}$ orbit coupled to the 2^+ state of ^{6}He. The $1/2^-$ resonance is calculated to be at 2.09 MeV resonance energy, i.e. 1.46 MeV excitation energy. Thus our results agree with the experiment of Ryezayeva *et al*[24] and possibly with Skaza *et al*[21] but not with other measurements. Other

theoretical calculations also do not lead to any unambiguous conclusion. Continuum shell model study[18] shows the ground state resonance $3/2^-$ at 0.36 MeV and the excited $1/2^-$ state around an excitation energy of 3.3 MeV. On the other hand, recoil corrected continuum shell model study of Halderson[26] place the resonance energy around 1 MeV.

3.2. Medium mass nuclei

In Table 3, we present our results for binding energy for neutron rich Ca and Ni isotopes and compare with RCHB calculation and also with experimental values wherever available. We see that the present calculated values compare favourably with the more elaborate and time consuming RCHB approach. One can also see that the experimental trend has been reproduced well. The last bound even-even nucleus corresponds to $A = 72$ and $A = 98$, respectively, in Ca and Ni isotopes. Does these correspond to any magic numbers?

A very important quantity is the pairing energy defined in the present calculation as E_p=BE(RMF+BCS)-BE(RMF). This is important for the study of the effect of closed shells. We plot our results in Figure 2. We see that in Ca isotopes, $N = 20$ and $N = 40$ are the magic numbers. For Ni isotopes magicity appears at $N = 40,\ 50$, and more importantly, at $N = 70$. A particularly interesting observation is that N=50 is no longer a magic number for Ca.

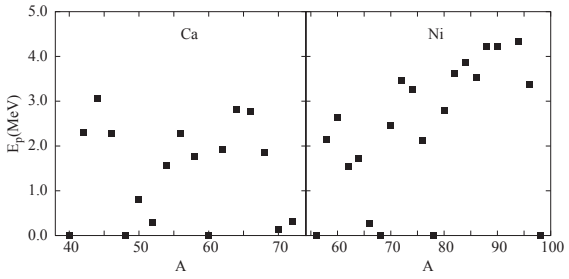

FIGURE 2. Pairing energy in RMF calculation in even Ca and Ni isotopes.

The calculated set of magic numbers can be explained on the basis of the single particle structures in neutron rich isotopes. The single particle levels calculated in the RMF method in these nuclei are shown in Figure 3.

In the neutron rich Ca isotopes, the $2d_{3/2}$, the $2d_{5/2}$ and the $3s_{1/2}$ levels come down in energy and approaches the $1g_{9/2}$ level. This effect has been seen in neutron rich nuclei in other mass regions also. The single particle levels in such nuclei often differ significantly from nuclei near the stability valley. In this particular instance, the dramatic relocation of the $3s_{1/2}$ state from the usual position at the top of the *sdg* shell near the stability valley to nearly the bottom of the shell is worth noting. The Fermi level, indicated by the solid line, rises very slowly near the drip line and finally becomes positive for ^{74}Ca. The states $1g_{7/2}$, $1h_{11/2}$, $2d_{3/2}$ and $2d_{5/2}$ remain resonant states in all the nuclei. The state $1g_{9/2}$ starts as a positive energy state but, as the neutron number increases, becomes loosely bound. Because of the absence of the centrifugal barrier, the level $3s_{1/2}$ does not have a resonant solution.

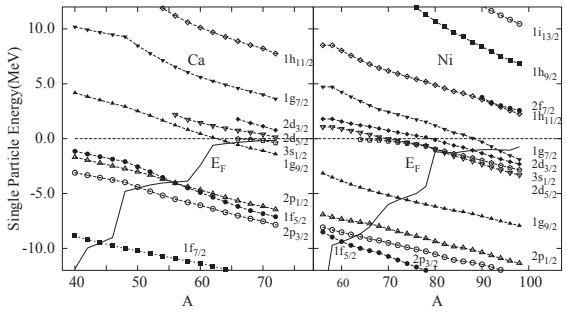

FIGURE 3. Single particle neutron energy in the RMF calculations in even Ca and Ni isotopes. The Fermi level is shown by the continuous line.

The disappearance of the magic gap at $N = 50$ in Ca nuclei is worth noting. The occupation probability v^2 and the pairing gap Δ values for the different states near the Fermi level in ^{70}Ca are shown in Figure 4. One can

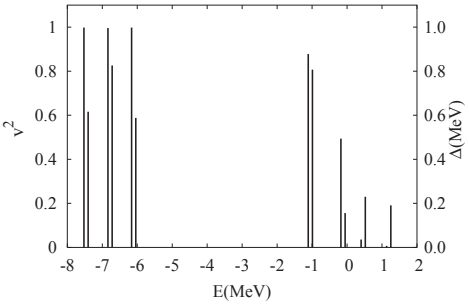

FIGURE 4. Occupation factor (v^2) and pairing gap (Δ) for single neutron states in ^{70}Ca plotted against the energy of the state. The left (right) axis and columns represents occupation factor (pairing gap) for different levels around the Fermi surface.

see that the large gap at $N = 40$ is persisting. However, among the states above the Fermi level, the occupancy of the $3s_{1/2}$ state is substantially large. We conclude that there is no shell closure at $N = 50$. The disappearance of the shell closure at $N = 50$ in neutron rich isotopes has earlier been observed in many theoretical studies. In a study of neutron rich Cr and Fe isotopes [28], we also have seen the same effect. However, in Figure 2

TABLE 3. Binding energy in MeV for neuron rich even Ca and Ni isotopes compared with experimental values. The RCHB results are from [27].

Element	A	RMF	RCHB	Expt	A	RMF	RCHB	Expt
	48	416.10	414.91	415.99	50	425.18	424.44	427.49
	52	433.79	433.22	436.59	54	441.83	441.35	444.10*
	56	449.62	449.00	449.79*	58	457.24	456.30	
Ca	60	464.68	463.26		62	465.96	465.32	
	64	466.88	466.56		66	467.56	467.32	
	68	468.01	467.75		70	468.30	467.96	
	72	468.35	467.99		74	468.04	467.64	
	68	591.20	589.51	590.41	70	603.66	602.09	602.21
	72	615.14	613.41	613.35	74	625.91	623.98	623.75
	76	636.06	634.01	633.16	78	645.60	643.61	641.94
	80	647.89	646.36		82	650.31	648.98	
Ni	84	652.74	651.49		86	655.20	653.85	
	88	657.39	656.04		90	659.42	658.03	
	92	661.35	659.85		94	663.27	661.57	
	96	665.17	663.22		98	667.07	664.78	
	100	663.99						

* Estimated value

one can still see a substantial drop in the pairing energy at $N = 50$, indicating the closure of the $1g_{9/2}$ subshell. Such a drop is also observed at $N = 32$ corresponding to the closure of $2p_{3/2}$ subshell. The calculated occupancy factors for the levels in the *sdg* shell in nuclei with $A > 60$ are give in Table 4. One can see that for $N = 52$, the occupancy of the $2d_{5/2}$ state is appreciable. This is the reason that contrary to Ref. [29], the pairing energy actually increases from ^{70}Ca to ^{72}Ca in our calculation. The states $1g_{9/2}$, $3s_{1/2}$, and $2d_{5/2}$ lie very close to each other in neutron rich Ca nuclei, thus no shell closure beyond N=40 is observed in Ca nuclei within the neutron drip line.

TABLE 4. The calculated occupancy (v^2) values in $^{62-72}$Ca isotopes for the states in the *sdg* shell. Also shown are the number of nucleons in the continuum (N_h).

	States					N_h
A	$1g_{9/2}$	$1g7/2$	$2d_{5/2}$	$2d_{3/2}$	$3s_{1/2}$	
62	0.207	0.002	0.004			2.11
64	0.405	0.002	0.008			0.064
66	0.592	0.003	0.013	0.004	0.026	0.118
68	0.764	0.003	0.022	0.006	0.120	0.180
70	0.878	0.003	0.036	0.007	0.495	0.268
72	0.949	0.003	0.114	0.008	0.895	0.740

In even Ni isotopes the Fermi level is deeper and abruptly becomes positive beyond A=98. The levels $3s_{1/2}$, $1g_{7/2}$, $2d_{3/2}$, and $2d_{5/2}$ lie very close to each other. All of them except the first start as positive energy states and become bound states at higher neutron number. The intruder orbit $1h_{11/2}$ lies much higher in energy. This is a consequence of the quenching of the spin orbit splitting in neutron rich nuclei which has been obtained in many mean field calculations and also experimentally observed in light nuclei. Thus $N = 70$ becomes a new magic number.

We have calculated the binding energy corresponding to the different single particle levels in odd nuclei. Although the ground state spin parity is unknown in many of the nuclei, we find that, except for ^{75}Ni, the spin parity has been correctly predicted wherever the ground state is unambiguously known. The striking features for these two chains of isotopes are the differences in the position of the drip line for odd and even isotopes. In Ca isotopes,

TABLE 5. Binding energy for neutron rich odd Ca and Ni isotopes in MeV compared with experimental values.

	B.E.(MeV)			B.E.(MeV)	
A	RMF	Expt	A	RMF	Expt
		Ca			
49	420.13	421.14	51	428.85	431.85
53	436.86	440.01	55	444.92	446.38
57	452.65	451.55	59	460.15	
61	464.26				
		Ni			
69	596.16	594.99	71	608.18	606.34
73	619.35	617.14	75	629.83	627.37
77	639.68	636.33	79	646.30	
81	648.70		83	651.15	
85	653.55		87	655.80	
89	657.87		91	659.62	
93	661.43		95	663.37	
97	665.28		99	665.03	

the last odd mass nucleus stable against neutron emission is ^{59}Ca while the corresponding even mass isotope is ^{72}Ca. On the other hand, the corresponding drip line nuclei in Ni are ^{97}Ni and ^{98}Ni, respectively. In other words, all the Ni isotopes are stable against neutron emission up

to $N = 70$ beyond which neither the even nor the odd isotopes are stable for this element. For Ca the odd isotopes are stable below $N = 40$ while stable even isotopes range up to $N = 52$.

The reason for this difference has been traced to the new magic numbers in neutron rich nuclei. As already pointed out, in Ca isotopes, the last neutron magic number is $N = 40$ and the magic gap at $N = 50$ vanishes. The single particle levels beyond $N = 40$ are either in the continuum or very loosely bound. Importantly, in Ca isotopes, the level $1g_{9/2}$ lies either in the continuum or just bound around N=40. Hence the stability of the isotopes depends crucially on the pairing interaction and the contribution of the states in the continuum. Thus the odd mass Ca isotopes beyond $N = 40$ are unstable against neutron emission. On the other hand, the Ni isotopes present a completely different picture. Here, $N = 70$ is a new magic number and the levels below it are bound by more than 2 MeV. Because of the comparatively larger binding energy, the binding energy of the odd nuclei does not depend overmuch on the pairing. Hence we obtain both even and odd mass nuclei which are stable against particle emission up to the new magic number N=70. A situation similar to Ca isotopes is expected in Zr where relativistic theories predict that the drip line for even Zr nuclei is around $N = 96$ but at $N = 77$ in odd isotopes due to pairing effects.

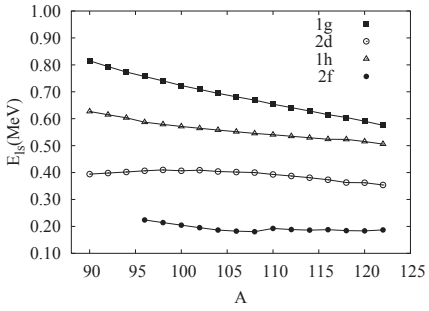

FIGURE 5. Spin orbit splitting in even Zr isotopes

One of the interesting predictions in neutron rich nuclei is this decrease in the spin-orbit splitting. Indeed it is particularly this effect that leads to the prediction and, in light nuclei, observation of emergence of new magic numbers along with disappearance of old ones. Though we have not studied the drip line for even even isotopes which, as we have observed, is far away form the isotopes we have studied, a decrease in the spin orbit splitting is already evident. In Fig. 5, we have plotted the splitting for these nuclei. Here we have defined $E_{ls} = |E_{l+1/2} - E_{l-1/2}|/(2l+1)$. It is clear that for high spin orbitals, the splitting falls off sharply with increase in the number of neutrons.

3.3. Scattering involving very light nuclei

One important problem in light nuclei is the interpretation of the radius. For a nucleus with only a few nucleons, the bulk radius value, extracted from experiment, may also be model dependent. Direct comparison with experimental measurements may yield better idea about the accuracy of the calculation. For example, calculation of differential cross section in elastic proton scattering in inverse kinematics is expected to provide a test for the calculated densities[30].

RMF calculations have been found to provide good description of densities, particularly at large radii. A good description of elastic scattering may be expected if we use microscopic nucleon-nucleon (NN) interactions and densities from RMF calculations to construct nucleon-nucleus potentials.

Effective NN interactions, such as density dependent M3Y (DDM3Y)[31, 32, 33], or that of Jeukenne, Lejeune and Mahaux (JLM)[34] may be used to construct the nucleon (nucleus)-nucleus potential. The DDM3Y interaction[31, 32] is obtained from a finite range energy independent M3Y interaction by adding a zero range energy dependent pseudopotential and introducing a density dependent factor. The density dependence was chosen in the form $C(1 - \beta\rho^{2/3})$[32]. The constants were obtained from nuclear matter calculation[33] as $C = 2.07$ and $\beta = 1.624$ fm^2. We have adopted all the standard parameters in our calculation without any modification. The real and the imaginary parts of the potential have been chosen as 0.8 times and 0.2 times the folded value for the DDM3Y potential. One can see that the experimental The JLM interaction was derived from the nuclear matter calculation [34] in the local density approximation by substituting the nuclear matter density with the calculated density distribution of the finite nucleus. Further improvement is incorporated in terms of the finite range of the effective interaction by including a Gaussian form factor. We have used the global parameters for the effective interaction and the respective default normalizations for the potential components from Refs. [35] and [36] with Gaussian range values of $t_{real} = t_{imag} = 1.2$ fm.

In Fig. 6, the measured partial cross sections for proton scattering of ^{6,8}He in inverse kinematics have been compared with theory. values are nicely reproduced. Similar results are obtained for many other light nuclei.

4. CONCLUSIONS

Neutron rich nuclei has been studied in RMF formalism with explicitly taking the effect of resonant continuum into account. We find that only a few positive energy resonant states along with the bound states are sufficient

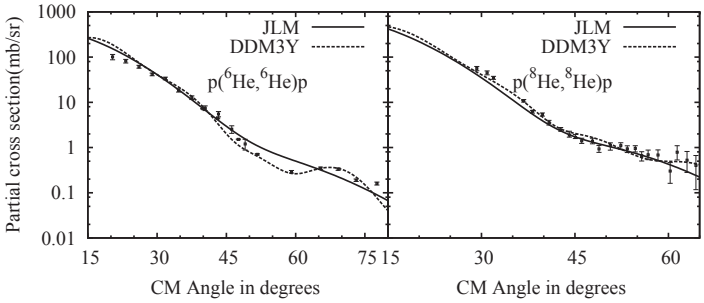

FIGURE 6. Partial cross section for the elastic proton scattering in inverse kinematics. The projectile energies of ^{6}He and ^{8}He are 71 MeV/A and 72 MeV/A, respectively. The experimental values for ^{6,8}He scattering from Refs. [37, 38] and [39], respectively.

to produce results comparable to the more complicated RCHB approach for the total quantities like binding energy, radius, two neutron separation energy, etc in most cases. Calculations reveal rearrangement of single particle levels leading to new magic numbers. pairing interaction is seen to play a major role near the drip line and away from shell closure. Elastic scattering cross sections in light neutron rich nuclei have been studied in microscopic optical model.

ACKNOWLEDGMENTS

The authors thank the University Grants Commission and the Board of Research in Nuclear Sciences, Department of Atomic Energy for financial support.

REFERENCES

1. See *e.g.* P. Ring, Prog. Part. Nucl. Phys. **37** 193 (1996).
2. M.M. Sharma, M.A. Nagarajan, and P. Ring, Phys. Lett. **312B**, 377 (2003).
3. G.A. Lalazissis, J. König, and P. Ring, Phys. Rev. C**55**, 540 (1997).
4. S. J. Lee *et al*, Phys. Rev. Lett. **57**, (1986).
5. J. Piekarewicz and B.G. Todd-Rutel, Phys. Rev. Lett. **95**, 122501 (2005).
6. M. Grasso, N. Sandulescu, N. Van Giai and R.J. Liotta, Phys. Rev. C **64**, 064321 (2001).
7. M. Grasso, N. Van Giai and N. Sandulescu, Phys. Lett. **B535**, 103 (2002).
8. N. Sandulescu, L.S. Geng, H. Toki and G.C. Hillhouse, Phys. Rev. C**68**, 054323 (2003).
9. L. Cao and Z.Y. Ma, Eur. Phys. Jour. **A 22**, 189 (2004).
10. G. Gangopadhyay, Phys. Rev. C. **59**, 2541 (1999)
11. G. Audi, A.H. Wapstra, and C. Thibault, Nucl. Phys. **A729**, 337 (2003).
12. C. Frossén, P. Navrátil, W.E. Ormand, and E. Caurier, Arxiv Nuc. Th. 0412049 (2004).
13. G.A. Lalazissis, D. Vretenar, and P. Ring, Eur. Phys. J. A **22**, 37 (2004).
14. Yu. Aksyutina *et al*, Phys. Lett. **B679**, 191 (2009).
15. K. Markenroth *et al*, Nucl. Phys. **A679**, 462 (2001).
16. D.R. Tilley *et al*, Nucl. Phys. **A 708**, 3 (2002).
17. See the compilation F. Ajzenberg-Selove, Nucl. Phys. **A 490**, 1 (1988).
18. A. Volya and V. Zelevinsky, Phys. Rev. C **74**, 064314 (2006).
19. A.F. Wuosmaa *et al*, Phys. Rev. C **78**, 041302(R) (2008) and references therein.
20. M. Meister *et al*, Phys. Rev. Lett. **88**, 102501 (2002).
21. F. Skaza *et al*, Phys. Rev. C **73**, 044301 (2006).
22. K. Markenroth, Nucl. Phys. **A679**, 462 (2001).
23. G.V. Rogachev, Phys. Rev. Lett. **92**, 232502 (2004).
24. Ryezayeva N *et al*2006 Phys. Lett. **B639** 623
25. A.F. Wuosmaa *et al*, Phys. Rev. C **72**, 061301(R) (2005).
26. D. Halderson, Phys. Rev. C **70**, 041603(R) (2004).
27. S.Q. Zhang, J. Meng, H. Toki, I. Tanihata, and S.-G. Zhou, Science in China **G46**, 632 (2003).
28. P. Mitra and G. Gangopadhyay, Int. Jour. Mod. Phys. E **13**, 1209 (2004).
29. H.L. Yadav, M. Kaushik and H. Toki, Int. Jour. Mod. Phys. E **13**, 647 (2004).
30. N. Alamanos and P. Roussel-Chomaz, Ann. Phys. Fr. **21**, 601 (1996).
31. A.M. Kobos, B.A. Brown, R. Lindsay, and G. R. Satchler, Nucl. Phys. **A425** 205 (1984)
32. A.K. Chaudhuri, Nucl. Phys. **A449**, 243 (1966); **A459**, 417 (1986).
33. D.N. Basu, J. Phys. G: Nucl. Part. Phys. **30**, B7 (2004).
34. J.P. Jeukenne, A. Lejeune, and C. Mahaux, Phys. Rev. C **14**, 1391 (1974).
35. E. Baugei, Commissariat a l'Energie Atomique, Bruyeres-Le-Chatel, France, v 1.01.
36. E. Bauge, J.P. Delaroche, and M. Girod, Phys. Rev. C **63**, 024607 (2001).
37. A.A. Korsheninnikov *et al*, Phys. Lett. **343B**, 53 (1995)
38. M. Hatano *et al*, Eur. Phys. J. **A 25**, 255 (2005).
39. A.A. Korsheninnikov *et al*, Phys. Lett. **B 316** 38 (1993).